DYNAMICS OF SMALL SPIN POLARON IN THE THREE-BAND MODEL OF TWO-DIMENSIONAL SPHERICALLY SYMMETRIC ANTIFERROMAGNET

A. F. Barabanov[a], R. O. Kuzian[b], L. A. Maksimov[c], E.Žasinas[a]

[a] *Institute for High Pressure Physics*
142092, Troitsk, Moscow Region, Russia
[b] *Institute for Materials Science*
252180, Kiev, Ukraine
[c] *Russian Research Center «Kurchatov Institute»*
123182, Moscow, Russia

The retarded Green's function $G(\mathbf{k}, \omega)$ of a single small spin polaron in the three-band model for the CuO_2 plane is calculated in the self-consistent Born approximation. It is shown that such a spin polaron is a good quasiparticle excitation for realistic values of spin exchange J and effective hopping τ. The polaron spectral density $A_p(\mathbf{k}, \omega)$ demonstrates small damping in contrast to the results of calculations starting from the bare hole, i.e., the pole strength $Z_p(\mathbf{k})$ of the energetically low-lying quasiparticle peak varies from 50% to 82% for $J/\tau \sim 0.1$–0.7. The quasiparticle peak dispersion reproduces the main features of the bare polaron spectrum $\Omega_{\mathbf{k}}$ near the band bottom. The spherically symmetric approach is used for the description of spin excitations. This approach makes it possible to consider the quantum antiferromagnetic background without the spontaneous symmetry breaking and the unit cell doubling. The new method of the self-consistent calculation, based on continuous-fraction expansion of the Green's function, is presented in detail. The method preserves the proper analytical properties of the Green's function and makes it possibile to analyze the nature of its singularities.

1. INTRODUCTION

The hole motion in a two-dimensional $(2D)$ $s = 1/2$ quantum antiferromagnet (AFM) has been studied in depth theoretically [1]. The important question is whether a hole injected in the undoped ground state behaves like a quasiparticle. This problem is mainly investigated within the framework of self-consistent Born approximation (SCBA) for the t–J model [2–7] and Kondo lattice [8]. There are only a few studies devoted to the three-band Hubbard model or the Emery model [9, 10] which is more realistic for CuO_2 planes in high-T_c superconductors (HTSC). For the t–J model it was shown that the spectral density function $A_h(\mathbf{k}, \omega)$ of a doped hole revealed a quasiparticle peak of intensity $Z_{\mathbf{k}} \approx J/t$ and a broad incoherent part that has a width of about $(6$–$7)t$. The quasiparticle band bottom corresponds to the momenta $\mathbf{k}_1 = (\pm\pi/2, \pm\pi/2)$. Similar results were obtained for the Emery model [11, 12]. Both the presence of a large incoherent part and small intensity of quasiparticle peak indicate that bare holes are rather poor elementary excitations even for $\mathbf{k}$ close to $\mathbf{k}_1$.

In order to investigate the hole motion in the t–J model one usually decouples the hole operator into a spinless fermion and an antiferromagnetic magnon operator. As a result, the zero approximation corresponds to the dispersionless band with zero energy of the hole. The hopping of the particle appears only due to the fermion–magnon scattering, which is treated by the usual perturbation method in $\mathbf{k}$-space. For this reason, we think that in this approach

the resulting quasiparticle pole in the fermion Green's function involves mainly a polaron with a large radius. A similar situation takes place in the usual treatment of a hole motion in the effective three-band model [11–13] and the Kondo-lattice model [8], when one starts from a bare hole, rather then from a magnetic polaron of a small radius.

In the framework of the effective three-band model we studied the spectral density function $A_p(\mathbf{k}, \omega)$ of a single small polaron, i.e., an excitation which at the outset takes into account a local hole–spin coupling. It is known that the simplest candidate for such a small polaron is an analog of the so-called Zhang–Rice singlet in CuO_4 plaquette [14, 15]. The mean-field spectrum Ω_k of this excitation has been studied extensively [15] and will be used as the zero approximation in our treatment. We shall consider the coupling of a small polaron to spin-wave excitations in SCBA for the corresponding two-time retarded Green's function $G(\mathbf{k}, \omega)$.

Our motivations to study $A_p(\mathbf{k}, \omega)$ and the corresponding quasiparticle band are the following. First, it is easy to show for the one-hole problem that the mean-field energy of the polaron Ω_k represents the center of gravity of the spectral function:

$$\Omega_k = \int\limits_{-\infty}^{\infty} \omega A_p(\mathbf{k}, \omega) d\omega. \tag{1}$$

This means that the minimum of Ω_k is the upper bound of the actual position for the quasiparticle band bottom. The SCBA, based on a bare hole Green's function, gives the minimum value of quasiparticle energy $\omega_h^{min} = -2.6\tau$ [12] for a typical value of copper–copper AFM exchange constant $J = 0.7\tau$. Here τ is a constant of the effective oxygen–oxygen hopping via an intervening copper site (note that our unit of energy is twice that of [12], $\tau = 2t$). As to the value of the small polaron mean field band bottom, it turns out to be substantially lower than ω_h^{min}, $\Omega_k = -3.17\tau$ for the same value of J/τ. We may conclude, therefore, that important local correlations are lost in SCBA when we start from the bare hole operators.

Second, we shall show that a small polaron represents the elementary hole excitation much more better than a bare hole dressed by magnons within the framework of SCBA. This is manifested by a relatively large intensity of a quasiparticle peak in our calculation.

Finally, the mean field spectrum Ω_k of the simplest small spin polaron explicitly depends on the state of the antiferromagnetic background. In the case of long-range order state, Ω_k demonstrates a flat band region close to the magnetic Brillouin zone boundary [15]. This region corresponds to the bottom of the band. Moreover, if one takes into account the direct oxygen–oxygen hopping, finite temperature, and a more complicated form for a small polaron wave function, then Ω_k reproduces the experimentally observed extended saddle point [16–20], which is directed along the line $(0, \pi) - (0, 0)$ [21]. Therefore, it seems important to ascertain whether the quasiparticle band reproduces the peculiarities of Ω_k dispersion. Using a very simple variant of the model, we shall determine below whether this is in fact the case.

The distinctive feature of our investigation is the consideration of the AFM copper spin subsystem in a spherically symmetric approach [22, 23]. Such an approach is most appropriate in treating the quantum $2D$ AFM at any finite temperature. As a result, the scattering of a spin polaron by spin excitations in the singlet spin background leads to the spectral function periodicity relative to the full Brillouin zone. Note that the conventional two-sublattice spin approach leads to periodicity relative to the magnetic (reduced) Brillouin zone [2–7, 12].

The paper is organized as follows. In Sec. 2 we give the derivations for the self-consistent equation for the Green's function in the case of the small polaron approach. In Sec. 3 we present the procedure that makes it possible to avoid the iterative solution of the self-consistent

equation for complex energies. The procedure is based on the continuous-fraction expansion of Green's function and makes it possible to calculate consequently the coefficients of the continuous-fraction expansion with the use of the quadrature method. In Sec. 4 we offer the termination of the continuous-fraction, which leads to the correct analytical properties of the resulting Green's function. Numerical results for the self-energies and spectral functions, the relation of our results to the previous approaches, and discussion are given in Sec. 5. In Sec. 6 we summarize the results. An Appendix contains some details of the approach which gives the expression for integrals over the spectral density in terms of the chain representation of the continuous fraction.

Some of our results were presented in a brief Report [24]. In this paper we present additional results, describe the new method, and give more details about the calculations.

2. EFFECTIVE HAMILTONIAN AND SMALL POLARON GREEN'S FUNCTION

Following [9, 10, 15], we adopt the Hamiltonian that corresponds to one-hole problem in the CuO_2 plane of the high-T_c superconductors:

$$\hat{H} = \tau \sum_{r, a_1, a_2, \sigma, \sigma'} c^\dagger_{r+a_1,\sigma} c_{r+a_2,\sigma'} \left(\frac{1}{2}\delta_{\sigma\sigma'} + 2s_{\sigma\sigma'}S_r \right) + \frac{J}{2} \sum_{r,g} S_r S_{r+g}, \tag{2}$$

where $a_1, a_2 = \pm g_x/2, \pm g_y/2$, $g = \pm g_x, \pm g_y$. Here and below $g_{x,y}$ are the basic vectors of a copper square lattice ($|g| \equiv 1$), $r + a$ are four vectors of the O sites nearest to the Cu site r, the operator $c^\dagger_\sigma$ creates a hole with the spin index $\sigma = \pm 1$ at the O site, $s_{\sigma\sigma'} = \sigma_{\sigma\sigma'}/2$, and the operator S represents the localized spin at the copper site. As mentioned above, τ is the integral of oxygen hole hoppings, which takes into account the coupling of the hole motion with copper spin subsystem, and J is the constant of the nearest neighbor AFM exchange between the copper spins.

It is well known that the most prominent feature of the Hamiltonian (2) is that the low-energy physics of hole excitations is described by the Bloch sums $\mathscr{B}^\dagger_{k,\sigma}$ based on one site small polaron operators $\mathscr{B}^\dagger_{r,\sigma}$

$$\mathscr{B}^\dagger_{k,\sigma} = \frac{1}{\sqrt{NK_k}} \sum_r e^{ikr} \mathscr{B}^\dagger_{r,\sigma}, \tag{3}$$

$$\mathscr{B}^\dagger_{r,\sigma} = \frac{1}{2} \sum_a (c^\dagger_{r+a,\sigma} Z^{\bar\sigma\bar\sigma}_r - c^\dagger_{r+a,\bar\sigma} Z^{\sigma\bar\sigma}_r), \tag{4}$$

$$K_k = \left\langle \frac{1}{N} \sum_{r,r'} e^{-ik(r-r')} \{\mathscr{B}_{r,\sigma}, \mathscr{B}^\dagger_{r',\sigma}\} \right\rangle = 1 + \left(C_g + \frac{1}{4} \right) \gamma_k.$$

Here and below $\{,\}$, $[,]$ stand for an anticommutator and commutator, respectively; $\langle ... \rangle \equiv$ $\equiv Q^{-1}\text{Tr}[e^{-\beta H}...]$, and $Q = \text{Tr}\,e^{-\beta H}$; $\beta = (kT)^{-1}$ is an inverse temperature; $\bar\sigma \equiv$ $\equiv -\sigma$; $Z^{\sigma_1\sigma_2}_r \equiv |\sigma_1\rangle\langle\sigma_2|$ are the Hubbard projection operators for Cu sites state, $\gamma_k =$ $= (1/4) \sum_g \exp(ikg)$, and $C_g = \langle S_0 S_g \rangle$.

To calculate the average for commutators and anticommutators such as K_k, we take into account that these expressions are reduced to the two-site or three-site spin correlation

functions. In principle, it is necessary to solve a self-consistent problem for hole and spin subsystems in order to find these correlation functions. However, in the limit of a small number of holes it is possible to ignore the reverse influence of the holes on the spin subsystem. We can then use the results of [22, 23], where the indicated spin correlation functions are calculated in the spherically symmetric approach for the spin subsystem. In particular, in this approach the three-site correlation functions can be expressed in terms of the two-site spin correlation functions, $C_r = \langle S_0 S_r \rangle$. We recall that due to the spherical symmetry $\left\langle S_i^\alpha S_j^\beta \right\rangle = \delta_{\alpha\beta} \left\langle S_i^\alpha S_j^\alpha \right\rangle = \frac{1}{3} \langle \mathbf{S}_i \mathbf{S}_j \rangle$, $\langle S_i^\alpha \rangle = 0$. Simultaneously, as $T \to 0$, the spin subsystem is described by a long-range-order state with finite effective magnetization m, $C_r(|\mathbf{r}| \to \infty) = m^2(-1)^{r_x + r_y}$; here the value of m is dictated by the Bose condensation of spin excitations at the antiferromagnetic vector $\mathbf{q}_0 = (\pi, \pi)$.

Note that $\mathscr{B}_{k,\sigma}^\dagger |L\rangle$ corresponds to the CuO$_2$ plane state with the total spin equal to $1/2$ if $|L\rangle$ is the singlet state. We treat $\mathscr{B}_{k,\sigma}^\dagger$ as a candidate for the elementary excitations operator and calculate the corresponding retarded two-time Green's function $G(\mathbf{k}, \omega)$ and spectral density

$$A_p(\mathbf{k}, \omega) = -\frac{1}{\pi} \operatorname{Im} G(\mathbf{k}, \omega + i0^+),$$

$$G(\mathbf{k}, \omega) = \langle \mathscr{B}_{\mathbf{k},\sigma} | \mathscr{B}_{\mathbf{k},\sigma}^\dagger \rangle_\omega \equiv -i \int\limits_{t'}^{\infty} dt e^{i\omega(t-t')} \langle \{ \mathscr{B}_{\mathbf{k},\sigma}(t), \mathscr{B}_{\mathbf{k},\sigma}^\dagger(t') \} \rangle. \tag{5}$$

Using the equations of motion, the retarded two-time Green's function $G(\mathbf{k}, \omega)$ can be expressed (see, for example, [25, 26]) in the following form, which is analogous to the Dyson's equation:

$$G^{-1}(\mathbf{k}, \omega) = G_0^{-1} - \Sigma(\mathbf{k}, \omega), \tag{6}$$

$$\Sigma(\mathbf{k}, \omega) = \langle \mathscr{R} | \mathscr{R} \rangle^{(irr)} = \langle \mathscr{R}_{\mathbf{k},\sigma} | \mathscr{R}_{\mathbf{k},\sigma}^\dagger \rangle - \langle \mathscr{R}_{\mathbf{k},\sigma} | \mathscr{B}_{\mathbf{k},\sigma}^\dagger \rangle \langle \mathscr{B}_{\mathbf{k},\sigma} | \mathscr{B}_{\mathbf{k},\sigma}^\dagger \rangle^{-1} \langle \mathscr{B}_{\mathbf{k},\sigma} | \mathscr{R}_{\mathbf{k},\sigma}^\dagger \rangle, \tag{7}$$

where

$$G_0 = (\omega - \Omega_\mathbf{k})^{-1}, \quad \mathscr{R}_{\mathbf{k},\sigma} = [\mathscr{B}_{\mathbf{k},\sigma}, \hat{H}] = \frac{1}{\sqrt{NK_\mathbf{k}}} \sum_\mathbf{r} e^{-i\mathbf{k}\mathbf{r}} \mathscr{R}_{\mathbf{r},\sigma}, \tag{8}$$

$$\mathscr{R}_{\mathbf{r},\sigma} = -4\tau \mathscr{B}_{\mathbf{r},\sigma} + \mathscr{R}_{\mathbf{r},\sigma}^\tau + \mathscr{R}_{\mathbf{r},\sigma}^J, \tag{9}$$

$$\mathscr{R}_{\mathbf{r},\sigma}^\tau = -\frac{\tau}{2}\sigma \left(\sum_{\mathbf{g},\mathbf{a},\sigma_1} \sigma_1 Z_\mathbf{r}^{\bar{\sigma}\sigma_1} c_{\mathbf{r}+\mathbf{g}+\mathbf{a},\bar{\sigma}_1} - \sum_{\mathbf{g},\mathbf{a},\sigma_1,\sigma_2} \sigma_2 Z_\mathbf{r}^{\bar{\sigma}\sigma_1} Z_{\mathbf{r}+\mathbf{g}}^{\sigma_1\sigma_2} c_{\mathbf{r}+\mathbf{g}+\mathbf{a},\bar{\sigma}_2} \right),$$

$$\mathscr{R}_{\mathbf{r},\sigma}^J = \frac{J}{4}\sigma \left(\sum_{\mathbf{g},\mathbf{a},\sigma_1} \sigma_1 (Z_\mathbf{r}^{\bar{\sigma}\sigma_2} Z_{\mathbf{r}+\mathbf{g}}^{\sigma_2\bar{\sigma}_1} - Z_{\mathbf{r}+\mathbf{g}}^{\bar{\sigma}\sigma_2} Z_\mathbf{r}^{\sigma_2\bar{\sigma}_1}) c_{\mathbf{r}+\mathbf{a},\sigma_1} \right), \tag{10}$$

$$\Omega_\mathbf{k} = \langle \{ \mathscr{R}_{\mathbf{k},\sigma}, \mathscr{B}_{\mathbf{k},\sigma}^\dagger \} \rangle = (\tau Q_\tau + J Q_J)/K_\mathbf{k}, \tag{11}$$

$$Q_\tau(\mathbf{k}) = -\frac{7}{2} - 8\left(\frac{1}{4} + C_\mathbf{g}\right)\gamma_\mathbf{k} + \left(\frac{1}{8} - C_\mathbf{g} + \frac{1}{2}C_{2\mathbf{g}}\right)\gamma_{2\mathbf{k}} + 2\left(\frac{1}{8} - C_\mathbf{g} + \frac{1}{2}C_\mathbf{d}\right)\gamma_{d\mathbf{k}},$$

$$Q_J(\mathbf{k}) = C_g(\gamma_k - 4).$$

Here and below $\mathbf{d} = \mathbf{g}_x + \mathbf{g}_y$, and $\gamma_{dk} = \cos(k_x g)\cos(k_y g)$.

Note that the expession (6) is formally exact. However, in contrast to the Dyson's equation for the causal Green's functions, the diagrammatic representation is absent for the self-energy part (7). We see from Eqs. (6) and (7) that the self-energy $\Sigma(\mathbf{k}, \omega)$, which accounts for the interaction effects, is expressed in terms of the higher-order Green's functions. One should notice, first, that the terms linear in $\mathscr{B}_{\mathbf{k},\sigma}$ do not contribute to the irreducible Green's function (7). Second, the lowest-order self-energy contribution is provided by the first term on the right-hand side of expression (7), while the second term leads to higher-order corrections. Following Ref. 7, we evaluate (7) with a proper decoupling procedure for the two-time correlation function $\langle \mathscr{R}_{\mathbf{k},\sigma}(t)\mathscr{R}_{\mathbf{k},\sigma}^\dagger(t') \rangle$. This procedure is equivalent to SCBA in a usual diagrammatic technique [7]. In our case this means that the two-time correlation function is decoupled into the spin–spin correlation function and the polaron–polaron correlation function. The adopted decoupling procedure preserves the main character of polaron site operator (4) — four hole site operators surround the copper spin operator. It can be represented schematically in the form

$$\left\langle Z_{r_1}(t)\left(\sum_{a_1} c_{r_2+a_1}(t)Z_{r_2}(t)\right)\left(\sum_{a_2} Z_{r_3}(t')c_{r_3+a_2}^\dagger(t')\right)Z_{r_4}(t')\right\rangle \simeq$$

$$\simeq \left\langle\left(\sum_{a_1} c_{r_2+a_1}(t)Z_{r_2}(t)\right)\left(\sum_{a_2} Z_{r_3}(t')c_{r_3+a_2}^\dagger(t')\right)\right\rangle\langle Z_{r_1}(t)Z_{r_4}(t')\rangle. \qquad (12)$$

We note that the more complex decoupling procedure was also tested by us; it did not qualitatively alter the results given by approximation (12). In the next step we project the polaron operators in (12) onto $\mathscr{B}_{k\sigma}$:

$$c_i(t)Z_j(t) \simeq \xi\mathscr{B}_{k\sigma}(t), \quad \xi = \left\langle \{c_i(t)Z_j(t), \mathscr{B}_{k,\sigma}^\dagger\}\right\rangle. \qquad (13)$$

Scince we calculate only the irreducible part of Green's function (7), the averages $\langle Z_{r_1}(t)Z_{r_4}(t')\rangle$ are transformed the to corresponding spin–spin correlation functions $\langle S_{r_1}^\alpha(t)S_{r_4}^\alpha(t')\rangle$. Collecting all terms, we have

$$\langle\mathscr{R}_{\mathbf{k},\sigma}(t)\mathscr{R}_{\mathbf{k},\sigma}^\dagger(t')\rangle \simeq N^{-1}\sum_q \frac{K_{\mathbf{k-q}}}{K_{\mathbf{k}}}\Gamma^2(\mathbf{k},\mathbf{q})\langle\mathscr{B}_{\mathbf{k-q},\sigma}(t)\mathscr{B}_{\mathbf{k-q},\sigma}^\dagger(t')\rangle\langle\mathbf{S}_{-\mathbf{q}}(t)\mathbf{S}_{\mathbf{q}}(t')\rangle, \qquad (14)$$

where

$$\Gamma(\mathbf{k},\mathbf{q}) = \tau\Gamma_\tau(\mathbf{k},\mathbf{q}) + \frac{J}{2}\Gamma_J(\mathbf{k},\mathbf{q}),$$

$$\Gamma_\tau(\mathbf{k},\mathbf{q}) = 4\gamma_{\mathbf{k-q}}\left(\frac{1+\gamma_{\mathbf{k-q}}}{2K_{\mathbf{k-q}}} - 1\right), \quad \Gamma_J(\mathbf{k},\mathbf{q}) = 4\gamma_\mathbf{q}\left[\left(\frac{3}{4} - C_g\right)\frac{4\gamma_{\mathbf{k-q}}}{3K_{\mathbf{k-q}}} - 1\right],$$

$$\langle\mathbf{S}_{-\mathbf{q}}(t)\mathbf{S}_\mathbf{q}(t')\rangle = \frac{1}{N}\sum_{r,r'} e^{i\mathbf{q}\cdot(\mathbf{r'}-\mathbf{r})}\langle\mathbf{S}_\mathbf{r}(t)\mathbf{S}_{\mathbf{r'}}(t')\rangle.$$

Using the spectral representation for the Green's functions, we obtain the following intermediate result for the self-energy:

$$\Sigma(\mathbf{k}, \omega) = \frac{1}{N} \sum_{\mathbf{q}} \frac{K_{\mathbf{k-q}}}{K_{\mathbf{k}}} \Gamma^2(\mathbf{k}, \mathbf{q}) \int\limits_{-\infty}^{\infty} \frac{d\omega_1}{\pi} \times$$

$$\times \int\limits_{-\infty}^{\infty} \frac{d\omega_2}{\pi} \frac{e^{\beta(\omega_1 + \omega_2)} + 1}{\left(e^{\beta\omega_1} + 1\right)\left(e^{\beta\omega_2} - 1\right)} \frac{\mathrm{Im}\left[G(\mathbf{k} - \mathbf{q}, \omega_1 + i0^+)\right]\mathrm{Im}\left[D(\mathbf{q}, \omega_2 + i0^+)\right]}{\omega - (\omega_1 + \omega_2) + i0^+}. \quad (15)$$

The spin excitation Green's function is [22, 23]

$$D(\mathbf{q}, \omega) = \langle S^z_{-\mathbf{q}} | S^z_{\mathbf{q}} \rangle = -\frac{8JC_{\mathrm{g}}}{3} \frac{1 - \gamma_{\mathbf{q}}}{\omega^2 - \omega_{\mathbf{q}}^2}, \quad (16)$$

where

$$\omega_{\mathbf{q}}^2 = -32J\alpha_1 C_{\mathrm{g}}(1 - \gamma_{\mathbf{q}})(2\Delta + 1 + \gamma_{\mathbf{q}}).$$

We ignore the influence of doped holes on copper spin dynamics and use the spin spectrum parameters calculated in Ref. 22 (the vertex correction $\alpha_1 = 1.7$, the spin excitations condensation part $m^2 = 0.0225$, and $\Delta = 0$ at $T = 0$).

As a result, we obtain the integral equation for the Green's function that always arises within the framework of SCBA:

$$G(\mathbf{k}, \omega) = \frac{1}{\omega - \Omega_{\mathbf{k}} - \Sigma(\mathbf{k}, \omega)}, \quad (17)$$

where

$$\Sigma(\mathbf{k}, \omega) = \frac{1}{N} \sum_{\mathbf{q}} M^2(\mathbf{k}, \mathbf{q}) \left[(1 + \nu_{\mathbf{q}})G(\mathbf{k} - \mathbf{q}, \omega - \omega_{\mathbf{q}}) + \nu_{\mathbf{q}}G(\mathbf{k} - \mathbf{q}, \omega + \omega_{\mathbf{q}})\right]. \quad (18)$$

Here $\nu_{\mathbf{q}} = 1/\left[\exp(\beta\omega_{\mathbf{q}}) - 1\right]$ is the Bose function and

$$M^2(\mathbf{k}, \mathbf{q}) = \frac{K_{\mathbf{k-q}}}{K_{\mathbf{k}}} \Gamma^2(\mathbf{k}, \mathbf{q}) \frac{(-4C_{\mathrm{g}})\left(1 - \gamma_{\mathbf{q}}\right)}{\omega_{\mathbf{q}}}. \quad (19)$$

The function $\Gamma(\mathbf{k}, \mathbf{q})$ corresponds to the bare vertex for the coupling between a spin polaron and a spin wave. It is known [27] that this vertex is substantially renormalized for $\mathbf{q}$ close to the AFM vector $\mathbf{q}_0 = (\pi, \pi)$. This renormalization is due to the strong interaction of a polaron with the condensation part of spin excitations that must be taken into account at the outset. As a result, the renormalized vertex $\tilde{\Gamma}(\mathbf{k}, \mathbf{q})$ must be proportional to $\sqrt{(\mathbf{q} - \mathbf{q}_0)^2 + L_s^{-2}}$ [27], where L_s is the spin–spin correlation length; $L_s \to \infty$ in case of a long-range-order state of the spin subsystem. Below we take this renormalization into account empirically by the substitution

$$\Gamma(\mathbf{k}, \mathbf{q}) \to \tilde{\Gamma}(\mathbf{k}, \mathbf{q}) = \Gamma(\mathbf{k}, \mathbf{q})\sqrt{1 + \gamma_{\mathbf{q}}}. \quad (20)$$

The introduced vertex correction is proportional to $|\mathbf{q} - \mathbf{q}_0|$ for $\mathbf{q}$ close to $\mathbf{q}_0$. We have used also the following two functions for the vertex correction, $\sqrt{1 + \gamma_{\mathbf{q}}^3}$ and $\sqrt{1 + \gamma_{\mathbf{q}}^5}$, and have obtained the results similar to those presented below. Note that the bare vertex leads to a dramatic decrease of the quasiparticle bandwidth.

3. SOLUTION OF THE INTEGRAL EQUATION

The equation (17) is usually solved by an iteration procedure. We propose here an alternative method, which is based on the continuous-fraction expansion of $G(\mathbf{k}, z)$:

$$G(\mathbf{k}, z) = \cfrac{b_0^2}{z - a_0-} \ \cfrac{b_1^2}{z - a_1-} \cdots \cfrac{b_n^2}{z - a_n-} \cdots, \quad a_n = a_n(\mathbf{k}), \quad b_n = b_n(\mathbf{k}), \tag{21}$$

where

$$b_0^2 = \int\limits_{-\infty}^{\infty} A_p(\mathbf{k}, \omega)d\omega = K_{\mathbf{k}}, \quad a_0 = \frac{1}{b_0^2} \int\limits_{-\infty}^{\infty} \omega A_p(\mathbf{k}, \omega)d\omega = \Omega_{\mathbf{k}}.$$

The coefficients $b_n, a_n, n > 0$ are related to the spectral density $A_p(\mathbf{k}, \omega)$ via the set of orthogonal polynomials $P_n(\omega)$, which satisfy the recurrence [28–32]:

$$\begin{aligned} P_{-1}(\omega) &= 0, \quad P_0(\omega) = 1, \\ P_{n+1}(\omega) &= (\omega - a_n)P_n(\omega) - b_n^2 P_{n-1}(\omega), \end{aligned} \tag{22}$$

and

$$a_n = \frac{\displaystyle\int\limits_{-\infty}^{\infty} \omega P_n^2(\omega)A_p(\mathbf{k}, \omega)d\omega}{\displaystyle\int\limits_{-\infty}^{\infty} P_n^2(\omega)A_p(\mathbf{k}, \omega)d\omega}, \tag{23}$$

$$b_{n+1}^2 = \frac{\displaystyle\int\limits_{-\infty}^{\infty} P_{n+1}^2(\omega)A_p(\mathbf{k}, \omega)d\omega}{\displaystyle\int\limits_{-\infty}^{\infty} P_n^2(\omega)A_p(\mathbf{k}, \omega)d\omega}. \tag{24}$$

Here we have used the nonnormalized form of the polynomials

$$\int\limits_{-\infty}^{\infty} P_n(\omega)P_s(\omega)A_p(\mathbf{k}, \omega)d\omega = \delta_{ns} \left(\prod_{m=1}^{m=n} b_m \right)^2.$$

Comparing Eqs.(21) and (17), we see that the self-energy $\Sigma(\mathbf{k}, z)$ is the continuous fraction similar to $G(\mathbf{k}, z)$. Thus we can introduce the spectral density

$$\rho(\mathbf{k}, \omega) = - \operatorname{Im} \left[\Sigma(\mathbf{k}, \omega + i0^+) \right] / \pi$$

and the set of polynomials $\Pi_n(\omega)$ with the recurrence analogous to (22):

$$\Pi_n(\omega) = (\omega - a_n)\Pi_{n-1}(\omega) - b_n^2 \Pi_{n-2}(\omega), \qquad \Pi_0(\omega) = 1, \quad \Pi_{-1}(\omega) = 0,$$

where

$$b_1^2 = \int\limits_{-\infty}^{\infty} \rho(\mathbf{k}, \omega)d\omega, \quad a_1 = \frac{1}{b_1^2} \int\limits_{-\infty}^{\infty} \omega\rho(\mathbf{k}, \omega)d\omega,$$

$$a_{n+1} = \frac{\int\limits_{-\infty}^{\infty} \omega\Pi_n^2(\omega)\rho(\mathbf{k}, \omega)d\omega}{\int\limits_{-\infty}^{\infty} \Pi_n^2(\omega)\rho(\mathbf{k}, \omega)d\omega}, \quad b_{n+1}^2 = \frac{\int\limits_{-\infty}^{\infty} \Pi_n^2(\omega)\rho(\mathbf{k}, \omega)d\omega}{\int\limits_{-\infty}^{\infty} \Pi_{n-1}^2(\omega)\rho(\mathbf{k}, \omega)d\omega}, \quad n \geq 1. \tag{25}$$

On the other hand, we have the following relation from Eq. (18):

$$\rho(\mathbf{k}, \omega) = \frac{1}{K_\mathbf{k}} \frac{1}{N} \sum_\mathbf{q} M^2(\mathbf{k}, \mathbf{q}) \left[(1 + \nu_\mathbf{q})A_p(\mathbf{k} - \mathbf{q}, z - \omega_\mathbf{q}) + \nu_\mathbf{q}A_p(\mathbf{k} - \mathbf{q}, z + \omega_\mathbf{q}) \right]. \tag{26}$$

Inserting the expression for $\rho(\mathbf{k}, \omega)$ in Eq. (25), we can express the coefficients a_{n+1} and b_{n+2} in terms of the integrals of the form

$$\int\limits_{-\infty}^{\infty} (\omega \pm \omega_\mathbf{q})^m \Pi_i^2 A_p(\mathbf{k} - \mathbf{q}, \omega)d\omega, \quad i \leq n, \quad m = 0, 1, \tag{27}$$

Now, the trick is that the polynomials in ω in the integrals (27) have the degree less than or equal to $2n + 1$. As it was proved by Nex [29], such integrals may be expressed in terms of the coefficients $\{a_0, \ldots, a_n, b_0 \ldots, b_n\}$. The details of such a procedure are presented in the Appendix. It turns out, therefore, that in SCBA we can recursively calculate pairs of coefficients a_{n+1}, b_{n+1} and obtain $\Sigma(\mathbf{k}, \omega)$ in the continuous-fraction form. Of course, we must calculate simultaneously the coefficients at all the chosen $\mathbf{k} + \mathbf{q}$ points in the first Brillouin zone. Below the chosen points correspond to a lattice of 32×32 unit cells. Our procedure allows us to avoid the iterative solution of Eq. (17) for complex energies.

4. TERMINATION OF THE CONTINUOUS FRACTION

The procedure outlined in the previous section would be efficient if after calculating a finite number of coefficients a_n, b_n, $n \leq n_0$, we could appropriately approximate that part (infinite in our case) of the continuous fraction T_{n_0} which has not been calculated. In other words, we rewrite the expression (21) in the form

$$G(\mathbf{k}, z) = \frac{b_0^2}{z - a_0-} \frac{b_1^2}{z - a_1-} \cdots \frac{b_{n_0}^2}{z - a_{n_0} - T_{n_0}(\mathbf{k}, z)} \tag{28}$$

and try to find a function $\tilde{T}_{n_0}$ (so-called «terminator») that is close to T_{n_0}.

Various ways to construct such approximations are described in the literature on the recursion method [29–31]. The asymptotic behavior of continuous-fraction coefficients is governed by the band structure and singularities of spectral density [31]. The main asymptotic

behavior depends on the band structure: $\{a_n\}$ and $\{b_n\}$ converge toward limits in the single band case and oscillate endlessly in a predictable way in the multiband case. Damped oscillations are created by isolated singularities. The main point here is that an isolated simple pole produces *exponentially* damped contribution in $\{a_n\}, \{b_n\}$, $n \to \infty$. For our case it means that the quasiparticle pole position and weight could be obtained with high accuracy from finite number of coefficients, and the asymptotic behavior determines the incoherent part of the spectrum. It is obvious that the spectrum we deal with has a lower bound and no upper bound. We can thus expect that coefficients will not converge to some finite values but will rather tend to infinity.

In Fig. 1 we represent the coefficients a_n and b_n as functions of n calculated according to the procedure described in the preceding section for two values of J ($J = 0.7\tau$ and $J = 0.1\tau$) and for $\mathbf{k} = (\pi/2, \pi/2)$. We see that the distinctive feature of this dependence is that for large n the coefficients a_n and b_n are linear functions of n. Accordingly, the slope for a_n coefficients is twice as large as the slope for b_n. The behavior of the coefficients may therefore be approximated as

$$b_n \approx \lambda_1 n + \lambda_2, \quad a_n \approx 2\lambda_1 n + \lambda_3, \quad \lambda_i = \lambda_i(\mathbf{k}), \quad n \gg 1. \tag{29}$$

It is interesting that the coefficients for t–J model have the analogous behavior when the slave-fermion Hamiltonian of this model [2] is treated in SCBA [4]. For $J = 0.4t$, $\mathbf{k} = (\pi/2, \pi/2)$ the coefficients a_n and b_n , which are governed by the relation analogous to (18), are shown in Fig. 2a.

Now we shall show that the same asymptotic expression (29) has the continuous-fraction expansion of incomplete gamma function which is written as [33]
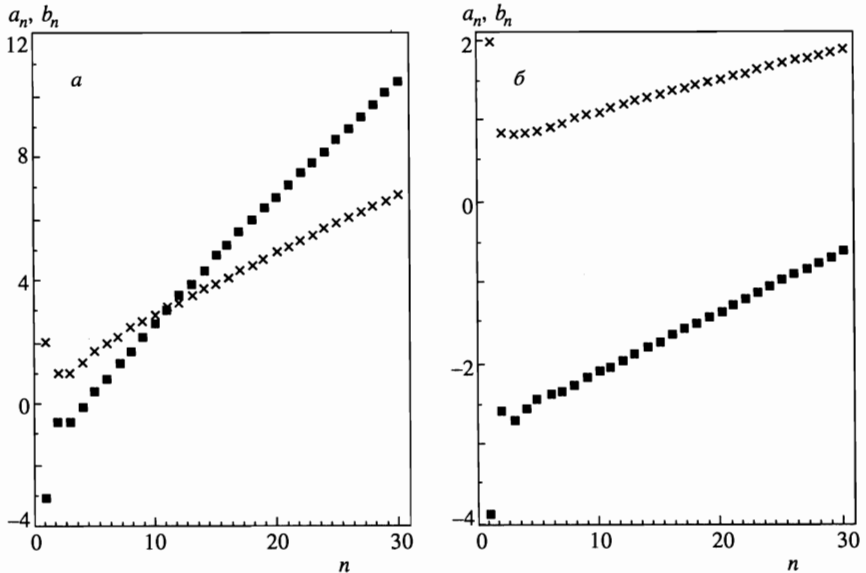
Fig. 1. The coefficients a_n (squares) and b_n (crosses) of the continuous-fraction expansion of $G_p(\mathbf{k}, \omega)$ as functions on n for $\mathbf{k} = (\pi/2, \pi/2)$: *a*) $J = 0.7\tau$; *b*) $J = 0.1\tau$. Calculated on the 32×32 cell lattice

$$\Gamma(\alpha, x) = \frac{e^{-x}x^{\alpha}}{x+} \frac{1-\alpha}{1+} \frac{1}{x+} \frac{2-\alpha}{1+} \cdots \tag{30}$$

We shall use this circumstance for the construction of the terminator $\tilde{T}_N(\mathbf{k}, z)$ for $G(\mathbf{k}, z)$ (28). We introduce the function

$$\tilde{g}(\alpha, x) = -\frac{\Gamma(\alpha, -x)}{e^x(-x)^{\alpha}} = \left(x - \frac{1-\alpha}{1-\theta_1}\right)^{-1}, \tag{31}$$

where

$$\theta_n = n\left(x - \frac{n+1-\alpha}{1-\theta_{n+1}}\right)^{-1}. \tag{32}$$

In order to rewrite the continuous fraction (31) in the form analogous to Eq. (21), we denote

$$\frac{1}{1-\theta_n} \equiv 1 + nt_n. \tag{33}$$

We can then obtain the relations

$$t_n = \frac{1}{x - (2n+1-\alpha) - (n+1)(n+1-\alpha)t_{n+1}}, \tag{34}$$

so that

$$\tilde{g}(\alpha, x) = t_0 \tag{35}$$

has the form (28) with the coefficients $\tilde{b}_0^2 = 1$ and

$$\tilde{a}_n = 2n + 1 - \alpha, \quad \tilde{b}_n^2 = n(n - \alpha). \tag{36}$$

Comparing Eqs. (29) and (36) for large n, when $\sqrt{n(n-\alpha)} \approx n - \alpha/2$, we see that the substitution

$$\alpha = -\frac{2\lambda_2}{\lambda_1}, \quad x = \frac{z + 2\lambda_2 - \lambda_3 + \lambda_1}{\lambda_1}$$

leads to the function $\tilde{G}$:

$$\tilde{G}(\mathbf{k}, z) = \frac{1}{\lambda_1} \tilde{g}\left(-\frac{2\lambda_2}{\lambda_1}, \frac{z + 2\lambda_2 - \lambda_3 + \lambda_1}{\lambda_1}\right), \tag{37}$$

which has the same asymptotic behavior as $G(\mathbf{k}, z)$ (Eq. (21)). This means that $\tilde{G}(\mathbf{k}, z)$ can be used as the terminator for $G(\mathbf{k}, z)$; i.e., we can express $\tilde{T}_{n_0}(\mathbf{k}, z) = \tilde{b}_{n_0+1}t_{n_0+1}$ in terms of $\tilde{G}(\mathbf{k}, z)$ and the coefficients $\tilde{a}_n$, $\tilde{b}_n$, $n \leq n_0$, and then substitute it for $T_{n_0}(\mathbf{k}, z)$ (see Ref. 30 for the details of matching Greenians).

We thus obtain $G(\mathbf{k}, z)$ in the whole complex energy plane including the real axis. Note that usually the procedure of discretizing the energy range ω is used for the iteration process when the Dyson's equation is solved numerically. It is not obvious that such a self-consistent solution leads to the correct analytical properties of the resulting Green's function. In contrast, the continuous-fraction representation guarantees these properties (e.g., the positive definiteness of spectral function $A_p(\mathbf{k}, \omega)$).

5. RESULTS AND DISCUSSION

In this section we present our results for the retarded Green's function $G(\mathbf{k}, \omega)$ for the three-band model at $T = 0$. The self-consistent equation (17) was solved on a 32×32 cell lattice. The number of calculated continuous-fraction levels n_0 was assumed to be $n_0 = 30$.

First, we check the validity of the method outlined above by calculating the spinless hole Green's function for the t–J model and compare the results with the results of Martinez and Horsch [4] obtained by the usual iteration procedure. In Fig.2 $A_h(\mathbf{k}_1, \omega + i\eta)$, $\mathrm{Re}\,\Sigma(\mathbf{k}_1, \omega)$, $-\,\mathrm{Im}\,\Sigma(\mathbf{k}_1, \omega)$, $\mathbf{k}_1 = (\pi/2, \pi/2)$ for the value of $J = 0.4t$ are represented for the 16×16 site lattice and broadening constant $\eta = 0.01t$. Comparison of Fig. 2b–d and the corresponding functions given in Figs. 7 and 8 from Ref. 4 (the same lattice size and the same η) demonstrates that the position of peaks of the hole spectral function and peak's intensities coincide. The difference is that our $A_h(\mathbf{k}_1, \omega)$ is more smooth and there are no strong oscillations in our self-energy $\Sigma(\mathbf{k}, \omega)$ in the interval $-2t < \omega < -0.75t$.

The results for the small spin polaron spectral density, real and imaginary parts of the self-energy for the characteristic value of energetic parameter $J = 0.7\tau$, are given in Fig. 3 for the symmetrical points $\mathbf{k}_1 = (\pi/2, \pi/2)$, $\mathbf{k}_2 = (0, 0)$, $\mathbf{k}_3 = (\pi, \pi)$. The energy broadening parameter is $\eta = 0.002$ (we will refer to all quantities in units of τ from now on). The main common feature in the spectral density for $\mathbf{k}_1$ and $\mathbf{k}_2$ is the existence of a sharp quasiparticle peak at the bottom of each spectrum. The position of the quasiparticle peak corresponds to the condition $\mathrm{Re}\,G^{-1}(\mathbf{k}, \omega) = 0$, i.e., the point where we have the crossing of the functions $y = \omega - \Omega_{\mathbf{k}}$ and $\mathrm{Re}\,\Sigma(\mathbf{k}, \omega)$, see Figs. 3a and 3b. In Fig. 3d we show $A_p(\mathbf{k}_1, \omega)$ calculated for $\eta = 0.002$ (solid line) and $\eta = 0.0005$ (dashed line) in order to study the scaling behavior of the peaks and their widths with respect to changes in η. Both peaks fit quite closely with a Lorentzian $(1/\pi)\left\{ Z(\mathbf{k}_1)\eta/\left[(\omega - \epsilon(\mathbf{k}_1))^2 + \eta^2\right]\right\}$, where $\epsilon(\mathbf{k}_1)$ is the location of the peak, which in the limit $\eta \to 0$ becomes $Z(\mathbf{k}_1)\delta(\omega - \epsilon(\mathbf{k}_1))$. This means that $\mathrm{Im}\,\Sigma(\mathbf{k}, \omega_p) \to 0$ in the same limit. Here and below we speak about the position $\epsilon(\mathbf{k})$ of such peaks (with the imaginary part of the pole close to zero) in terms of the quasiparticle energy.

Figures 3a and b also demonstrate that the incoherent part of $A_p(\mathbf{k}, \omega)$ increases and the pole strength decreases with the increasing of $\epsilon(\mathbf{k})$, $Z(\mathbf{k}_1) = 0.82$, $Z(\mathbf{k}_2) = 0.347$. We recall that $\Omega_{\mathbf{k}}$ represents the center of gravity of the spectral function. In our figures the center of gravity corresponds to the crossing of the real axis by the line $y = \omega - \Omega_{\mathbf{k}}$. Therefore, if the quasiparticle peak is far from this point, we would have a large incoherent part.

Quite different features are demonstrated in $A_p(\mathbf{k}_3, \omega)$ in Fig. 3c. The broad lowest peak is determined by the appearance of nonzero $\mathrm{Im}\,\Sigma(\mathbf{k}_3, \omega)$ in the region where $\mathrm{Re}\,G^{-1}(\mathbf{k}_3, \omega)$ has no zeros. Two broad additional peaks at $\omega \approx -1.6$ and $\omega \approx -1.05$ are formed due to the zero values of $\mathrm{Re}\,G^{-1}(\mathbf{k}_3, \omega)$ close to these ω. At the same time, the $\mathrm{Im}\,\Sigma(\mathbf{k}_3, \omega)$ is strong in these regions. Moreover, the maximum of $\mathrm{Im}\,\Sigma(\mathbf{k}_3, \omega)$ (near the point $\omega \approx -1.37$) determines the local minimum of $A_p(\mathbf{k}_3, \omega)$, despite of the fact that this point is close to the frequency where $\mathrm{Re}\,G^{-1}(\mathbf{k}_3, \omega) = 0$. It is clear that it is impossible to treat any of the $A_p(\mathbf{k}_3, \omega)$ peaks as a quasiparticle peak. Bear in mind that the qualitative behavior of the real part of the self-energy in Fig. 3c is close to that one which is represented by Kampf and Schrieffer; see Fig. 3b in Ref. 34, for the pseudogap regime of the Hubbard model. Figure 3c gives three solutions of $\mathrm{Re}\,G^{-1}(\mathbf{k}_3, \omega) = 0$. Although there is a sharp crossover from a situation with three solutions to one quasiparticle solution, the spectral function still changes smoothly due to the presence of the imaginary part of Σ.

Figures 3b and 3c demonstrate qualitatively a different character of $A_p(\mathbf{k}, \omega)$ for the points
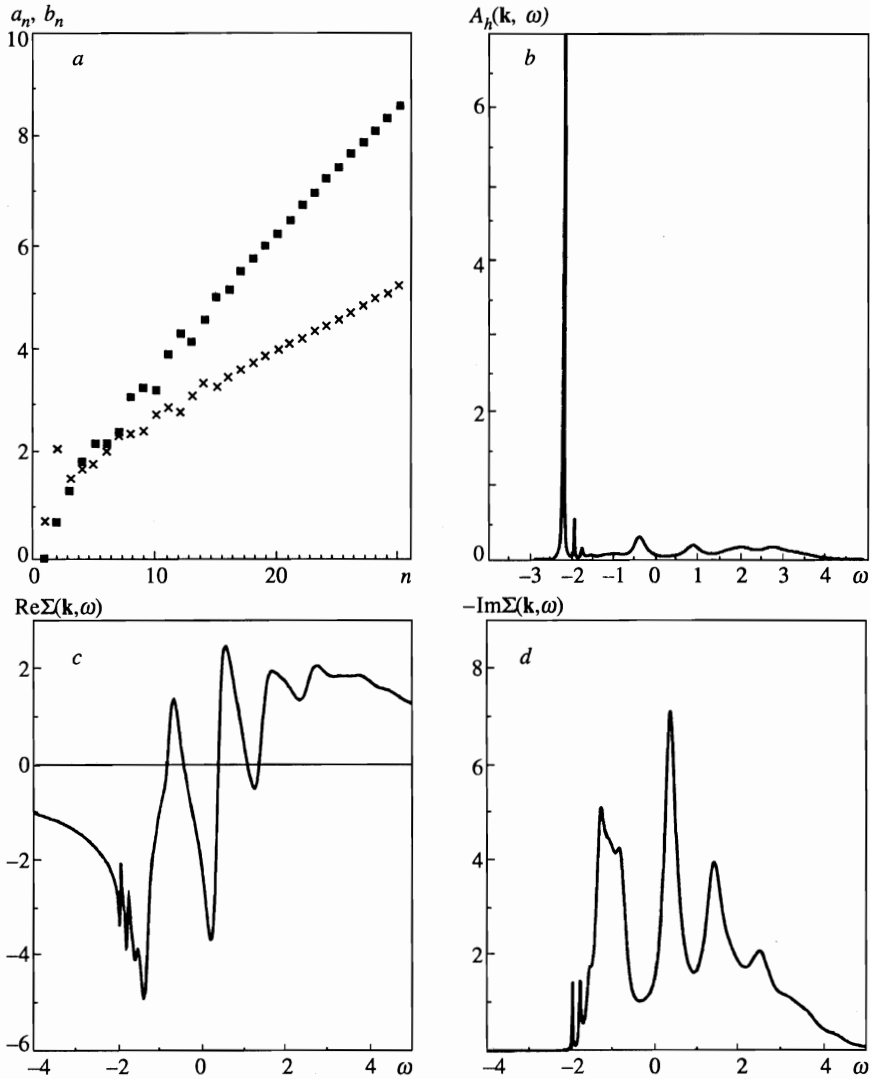
Fig. 2. Results for the hole Green's function $G_h(\mathbf{k}, \omega)$ for the t–J model calculated with the same parameters as in Ref. 4 ($J = 0.4t$, $\mathbf{k} = (\pi/2, \pi/2)$, $\eta = 0.01$, 16×16 site lattice): a) the coefficients a_n (squares) and b_n (crosses) of the continuous-fraction expansion of $G_h(\mathbf{k}, \omega)$ as functions of n; b) spectral function $A_h(\mathbf{k}, \omega)$; c) real part of the self-energy; d) imaginary part of the self-energy. The unit of energy is $t = 1$

$\mathbf{k}_2 = (0, 0)$, $\mathbf{k}_3 = (\pi, \pi)$. This is the consequence of the spherically symmetric approach in treating the AFM copper spin subsystem. As mentioned in the Introduction, this approach gives rise to the spectral function periodicity relative to the full Brillouin zone, not the magnetic zone.
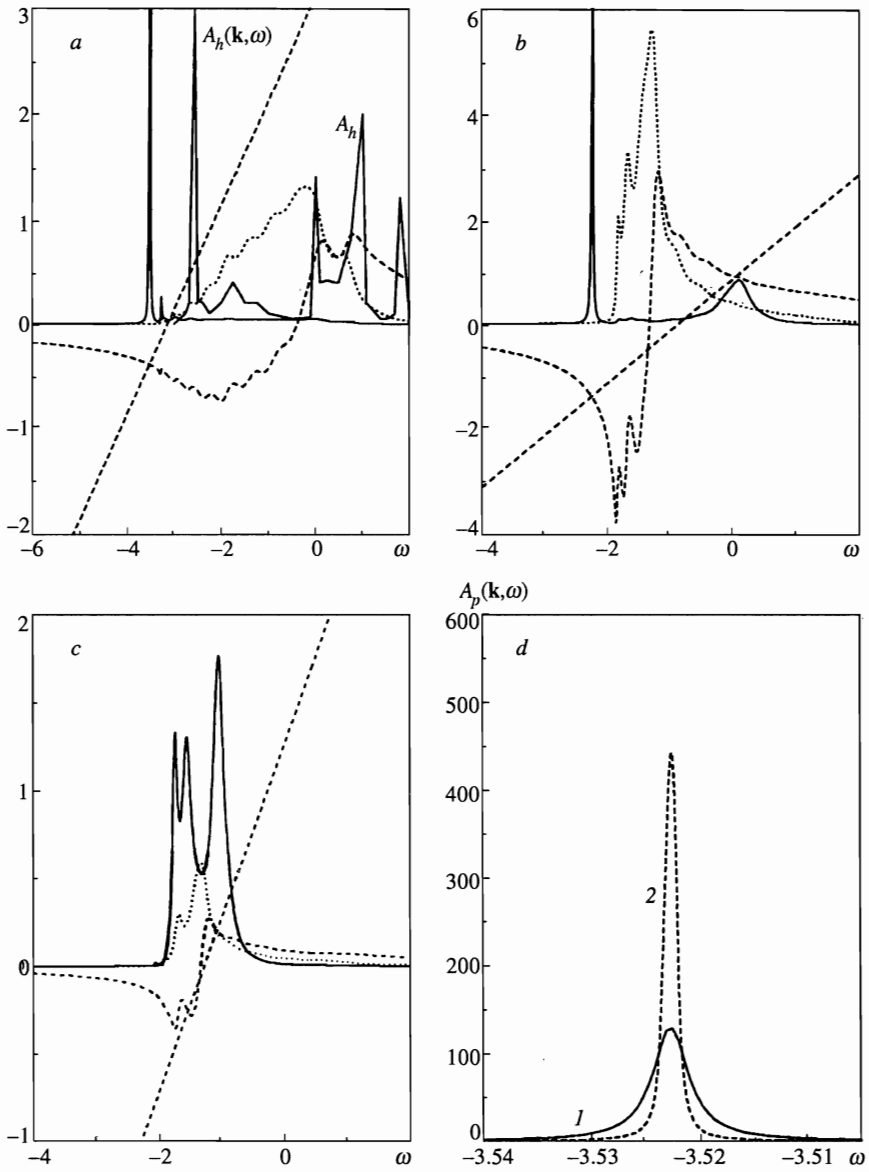
Fig. 3. Spin polaron spectral density ($A_p(\mathbf{k}, \omega)$, solid lines), real ($\operatorname{Re} \Sigma(\mathbf{k}, \omega)$, dashed lines) and imaginary ($-\operatorname{Im} \Sigma(\mathbf{k}, \omega)$, dotted lines) parts of the self-energy calculated for $J = 0.7\tau$, 32×32 cell lattice, and different $\mathbf{k}$: *a*) $\mathbf{k} = (\pi/2, \pi/2)$, here we also reproduce the hole spectral function $A_h(\mathbf{k}, \omega)$, which was obtained in Ref. 12; *b*) $\mathbf{k} = (0, 0)$; *c*) $\mathbf{k} = (\pi, \pi)$. In Fig. 1*a*–*c* $\eta = 0.002\tau$, the sloping straight lines represent the function $\omega - \Omega_{\mathbf{k}}$. *d*) The dependence of the quasiparticle peak of $A_p(\mathbf{k} = (\pi/2, \pi/2), \omega)$ for two values of the broadening factor η: *1* — $\eta = 0.02$; *2* — $\eta = 0.0004$. The unit of energy is $\tau = 1$
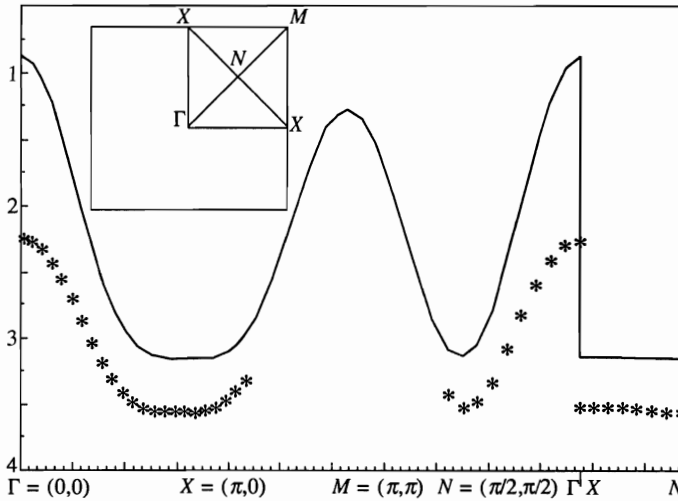
Fig. 4. The dispersion of the quasiparticle band $\epsilon(\mathbf{k})$ (symbols) and the mean field dispersion $\Omega_\mathbf{k}$ (solid line) along the symmetry lines in the Brillouin zone (see the inset) for $J = 0.7$, 32×32 cell lattice, and $\eta = 0.002$

In Fig. 4 we show the dispersion relation $\epsilon(\mathbf{k})$ of the quasiparticle band and the mean field dispersion $\Omega_\mathbf{k}$ along the symmetry lines in the Brillouin zone. For $\epsilon(\mathbf{k})$ we reproduce only those $\mathbf{k}$ values for which the lowest peak has a pronounced quasiparticle peak, taking into account the following criteria: $-\operatorname{Im}\Sigma(\mathbf{k}, \epsilon(\mathbf{k}) + i\eta) < 2\eta$, $\eta = 0.002$. As we know [15], due to the antiferromagnetic character of the spin correlation functions the $\Omega_\mathbf{k}$ demonstrates a «flat dispersion region» close to the line $\gamma_\mathbf{k} < 0, |\gamma_\mathbf{k}| \ll 1$, i.e., close to the boundary of the magnetic Brillouin zone X–N–X (see Fig. 4). As we see from Fig. 4, the quasiparticle band exists in the greater part of the Brillouin zone except the region at the top of the $\Omega_\mathbf{k}$ spectrum. Moreover, the dispersion law $\epsilon(\mathbf{k})$ qualitatively reproduces the main features of the spectrum $\Omega_\mathbf{k}$. As we mentioned in the Introduction, $\Omega_\mathbf{k}$ demonstrates the important features of the hole spectrum for CuO_2 plane if one takes into account the O–O hoppings and spin frustration [21]. We hope that in this case $\epsilon(\mathbf{k})$ will reproduce these features also.

Let us compare the small polaron spectral density $A_p(\mathbf{k}, \omega)$ with the results for the bare hole $A_h(\mathbf{k}, \omega)$ given by Kabanov and Vagov [12] for $\mathbf{k}_1 = (\pi/2, \pi/2)$, $J = 0.7\tau$ (see Fig. 3a). First, Fig. 3a indicates that $A_p(\mathbf{k}_1, \omega)$ has much sharper quasiparticle peaks relative to the results for a bare hole. For example, the pole strength $Z_p(\mathbf{k}_1)$ for the quasiparticle peak of $A_p(\mathbf{k}, \omega)$ is $Z_p(\mathbf{k}_1) = 0.82$. The corresponding value for A_h given by Ref. 12 is much smaller, $Z_h(\mathbf{k}_1) = 0.25$.

Second, Fig. 3a explicitly demonstrates the one-peak structure of $A_p(\mathbf{k}_1, \omega)$ in contrast to $A_h(\mathbf{k}_1, \omega)$. Finally, it is important that the bottom of our quasiparticle band $\epsilon(\mathbf{k}) = -3.52$ is substantially lower than $\omega_h^{min} = -2.6$ from Ref. 12. These results are the consequence of the fact that elementary excitation, i.e., spin polaron $\mathscr{B}_{\mathbf{k},\sigma}$, of small radii from the beginning involves the strong local hole–spin coupling.

It is clear that the quasiparticle peaks for a bare hole and a small polaron must coincide in the exact solution of the problem. The above mentioned discrepancies between our calculations and those of Ref. 12 are the consequence of different approximations.
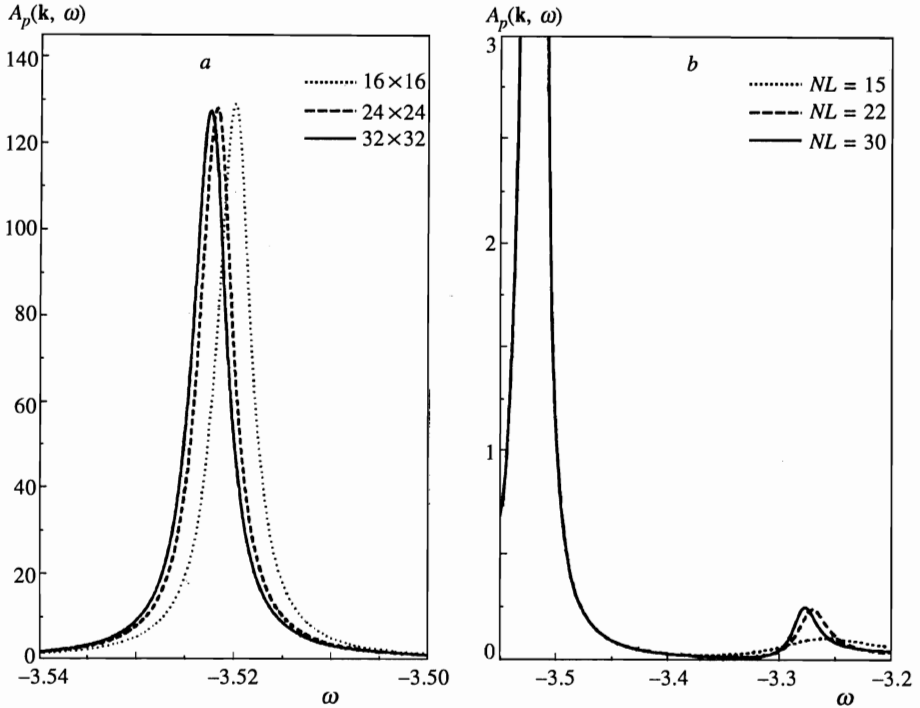
Fig. 5. The function $A_p(\mathbf{k} = (\pi/2, \pi/2), \omega)$ for $J = 0.7$ and $\eta = 0.002$ calculated for a) $NL = 30$ and different lattice sizes; b) 32×32 cell lattice and different numbers NL of calculated continuous-fraction levels

In order to test the convergence of our results relative to the increase of the lattice size and the number NL of calculated continuous-fraction levels, in Fig. 5 we show the quasiparticle peak of $A_p(\mathbf{k}, \omega)$ at $\mathbf{k} = (\pi/2, \pi/2)$, $J = 0.7$ for different lattices and n_0. This peak, as is evident from Fig. 5(a and b), changes insignificantly in going from 24×24 to 32×32 cell lattice and from $NL = 22$ to $NL = 30$.

We consider now the transformation of $G(\mathbf{k}, \omega)$ with the decrease of J. In order to clarify how the character of the $A_p(\mathbf{k}, \omega)$ peaks is changed, in Fig. 6 we show $A_p(\mathbf{k}, \omega)$ for the value of $J = 0.1$ at points $\mathbf{k}_1 = (\pi/2, \pi/2)$, $\mathbf{k}_2 = (0, 0)$, and $\mathbf{k}_3 = (\pi, \pi)$. The decrease of J leads to the enlargement of the broad, incoherent part of $A_p(\mathbf{k}, \omega)$.

As before, the flat band region of the quasiparticle band bottom enlarges along a magnetic Brillouin zone boundary. It is represented by the point $\mathbf{k}_1$. In Fig. 6a $A_p(\mathbf{k}_1, \omega)$ demonstrates explicitly a rather strong quasiparticle peak, $Z_p(\mathbf{k}_1) = 0.5$, which corresponds to the condition $\operatorname{Re} G^{-1}(\mathbf{k}, \omega) = 0$. Quite different character of $A_p(\mathbf{k}, \omega)$ is typical for $\mathbf{k}$ that correspond to the tops of $\Omega_\mathbf{k}$ band: in the low-energy sector for $\mathbf{k}_2, \mathbf{k}_3$ (see Figs. b and 6c) one observes $A_p(\mathbf{k}, \omega)$ peaks with small intensity. For example, the pole strength Z_p of such a quasiparticle peak for $A_p(\mathbf{k}_2, \omega)$ is $Z_p(\mathbf{k}_2) = 0.016$. Assuming $\omega_l(\mathbf{k})$ to be the value of ω corresponding to the center of these lowest in energy peaks, we see that $\operatorname{Re} G^{-1}(\mathbf{k}, \omega_l(\mathbf{k})) \neq 0$ for the $\mathbf{k}$ under discussion. Figures 6b and 6c demonstrates that these peaks are determined by the peaks in $\operatorname{Im} \Sigma(\mathbf{k}, \omega)$ at points $\omega_l(\mathbf{k})$. The self-energy part $\Sigma(\mathbf{k}, \omega)$ occurs through the Green's function of a small polaron bounded to spin waves. These peaks can be considered as the quasiparticle band of
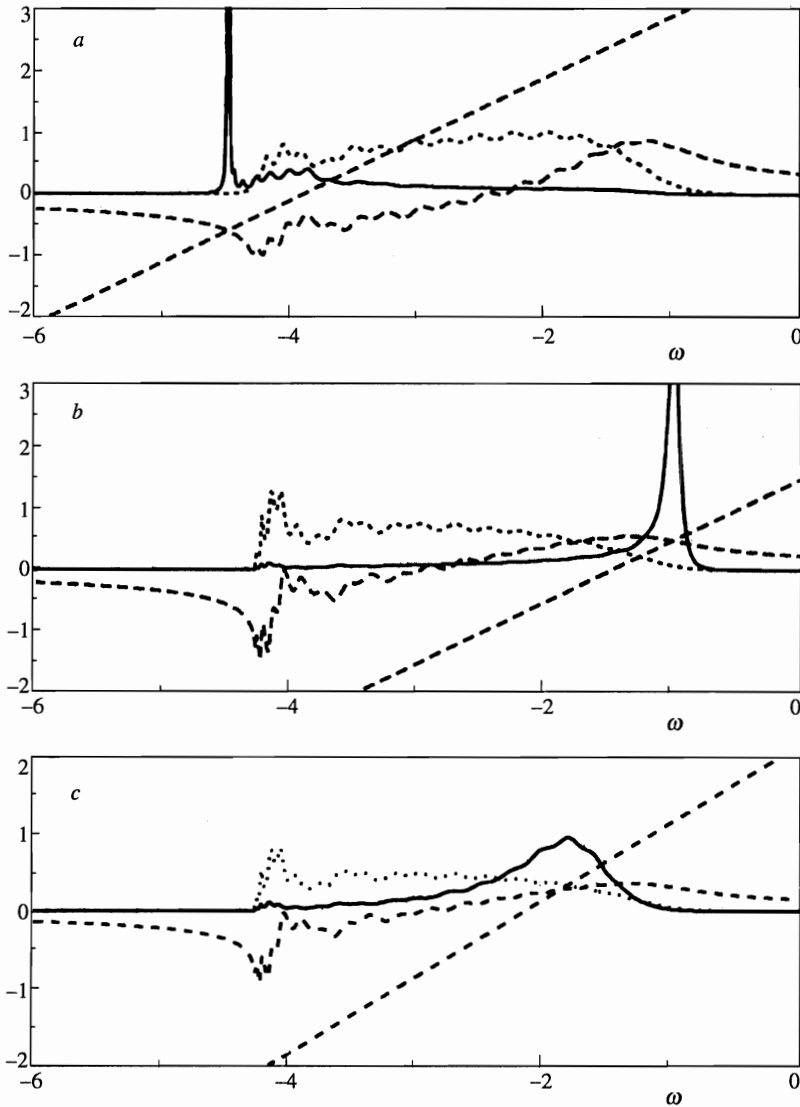
Fig. 6. Spin polaron spectral density ($A_p(\mathbf{k}, \omega)$ solid lines), real ($\mathrm{Re}\,\Sigma(\mathbf{k}, \omega)$, dashed lines) and imaginary ($-\mathrm{Im}\,\Sigma(\mathbf{k}, \omega)$, dotted lines) parts of the self-energy $\Sigma(k, \omega)$ calculated for $J = 0.1\tau$, $\eta = 0.002$, 32×32 cell lattice at three different $\mathbf{k}$: *a*) $\mathbf{k} = (\pi/2, \pi/2)$; *b*) $\mathbf{k} = (0, 0)$; *c*) $\mathbf{k} = (\pi, \pi)$

such complex states.

If we treat the width W of the quasiparticle band as the difference $\omega_l(\mathbf{k}_2 = (0, 0)) - \omega_l(\mathbf{k}_1 = (\pi/2, \pi/2))$, then W turns out to be of the order of J for small values of J ($J \simeq 0.1$), consistent with the results for the hole Green's function approach [12].

It is clear that for small J/τ the concept of a small spin polaron fails and it is important to estimate the validity limits of this concept. Our calculations demonstrate that the intensity

of quasiparticle peaks and the structure of $A_p(\mathbf{k}, \omega)$ do not change dramatically for $\mathbf{k}$, which corresponds to the band bottom, up to $J/\tau = 0.1$. For example, $Z_p(\pi/2, \pi/2) \approx Z_p(\pi, 0) \approx$ ≈ 0.50 at $J/\tau = 0.1$. Therefore, the J/τ lowest boundary value of the small spin polaron concept validity is lower than $J/\tau = 0.1$.

Table presents the numerical values $\omega_l(\mathbf{k})$ of the center position of the lowest $A_p(\mathbf{k}_2, \omega)$ peaks ($\omega_l(\mathbf{k}) = \epsilon(\mathbf{k})$ for $\mathbf{k}$ values where quasiparticle peak is observed) and their pole strength (area under the peak) $Z_p(\mathbf{k})$ for $\mathbf{k} = (\pi/2, \pi/2), (0, 0), (0, \pi)$ and different values of J.

Table 1

Position $\omega_l(\mathbf{k})$ of the lowest in energy peak and the area $Z_p(\mathbf{k})$ under the peak for different values of J/τ and k

J/τ	$Z_p(0,0)$	$\omega_l(0,0)$	$Z_p(\pi/2, \pi/2)$	$\omega_l(\pi/2, \pi/2)$	$Z_p(\pi, 0)$	$\omega_l(\pi, 0)$
0.1	0.016	−4.24	0.50	−4.48	0.55	−4.51
0.3	0.039	−3.37	0.72	−4.09	0.714	−4.13
0.5	0.174	−2.714	0.793	−3.79	0.738	−3.83
0.7	0.347	−2.25	0.823	−3.52	0.808	−3.56

We do not represent the results for large J ($J \gg \tau$) as our approach in the present form fails to describe this limit. Here, from the very beginning we treat a small polaron by a single site operator $\mathscr{B}_{\mathbf{r}, \sigma}$ (4). For large J the mean field static energy of such a state is proportional to J and such a state is unstable. In this limit, therefore, we must extend the basis of the site operators. The simplest way to do this is to include in the basis the additional operator of a bare hole. In SCBA this will lead to the system of two self-consistent equations. As a result, all effects of interaction between a spin subsystem and holes will be proportional to τ/J. The more general procedure for the extending of the small polaron operator basis is outlined in Ref. 21.

6. SUMMARY

We have studied the small spin polaron motion in the three-band model. The two-time retarded Green's function was calculated in the framework of self-consistent Born approximation for 32×32 cell lattice. We have shown that spin polaron of small radius represents a good approximation of the true quasiparticle low-energy excitation even at the mean-field level. Allowance for the self-energy does not crucially change the polaron motion picture for realistic values of parameters. For quasimomenta $\mathbf{k}$ values, which correspond to the band bottom, most of the total spectral weight is concentrated in the quasiparticle peak (Table 1). In the same region of $\mathbf{k}$-space the shape of the quasiparticle dispersion curve $\epsilon(\mathbf{k})$ reproduces the shape of the mean-field dispersion $\Omega_\mathbf{k}$ (Fig. 4).

We compared our results with the previous studies [11, 12] which started from the bare hole. We see that the small polaron mean-field energy $\Omega_\mathbf{k}$ lies much lower than the quasiparticle pole obtained from SCBA for the bare hole. Since $\Omega_\mathbf{k}$ determines the center of gravity for the Green's function spectral density, the actual quasiparticle pole position (at least for the band bottom) should lie deeper in energy than $\Omega_\mathbf{k}$ (Figs. 3 and 6). This means that in the three-band model the important local correlations should be taken into account in zero approximation and

small spin polaron should be constructed. The polaron scattering on spin waves will then be of less importance and it may be treated by perturbation methods.

We conclude that the low-energy physics of high-T_c superconductors should be considered in terms of small spin polaron dynamics. In particular, the problem of superconducting hole pairing must be treated as pairing of these quasiparticles rather than pairing of bare holes.

Finally, we wish to clarify the difference between our the approach and those that use a Neel-type spin subsystem state. Our calculations are based on approach developed in Refs. 22 and 23, where it is shown that a two-dimensional $s = 1/2$ antiferromagnetic system at low temperature is in the rotationally invariant state that preserves this invariance in the limit where T goes to zero and correlation length goes to infinity. Then, even for $T = 0$, the points $(0,0)$ and (π, π) are not equivalent due to the numerator in the spin Green's function (see Eq. (16)). As a result, the short-range spin–spin correlation functions, such as $C_{r,R}^{+-} = \langle S_r^+ S_{r+R}^- \rangle$, do not depend on the site r. Let us note that according to Marshall's theorem [35] the ground state of an antiferromagnet may be a spherically symmetric singlet state in the limit $N \to \infty$. The question about the ground state of a two-dimensional $s = 1/2$ AFM system is not established exactly. Since at any finite temperature the rotationally invariant theory is true for the paramagnetic system with strong short-range AFM correlations, we think that it is impossible for the system to undergo an abrupt transition to a state with a spontaneously broken symmetry at $T = 0$. Such a transition would mean an abrupt rise of the r-dependence in $C_{r,R}^{+-}$ and finite $\langle S_r^z \rangle$. We believe that the ground state of a two-dimensional $s = 1/2$ AFM system is a spherically symmetric state with the long-range order, and that it does not lead to the symmetry of the reduced antiferromagnetic zone. The energy bands therefore are change infinitesimally as we go from $T = 0$ to a temperature that is infinitesimally above zero.

In addition, our results demonstrate that the nonequivalence of the $(0,0)$ and (π, π) points for the spectral function $A(\mathbf{k}, \omega)$ and $\Omega_\mathbf{k}$ do not contradict the exact diagonalization studies for the ground state of the t–J model (see, e.g., Figs. 18a and 23 in Ref. 1).

A few words about the scenario which assumes that a smooth transition from rotationally invariant state to the state with spontaneously broken symmetry takes place. Such a transition implies a smooth increase in $\langle S_r^z \rangle$ and r-dependence of $C_{r,R}^{+-}$. The main effect consists not in the changes of $\Omega_\mathbf{k}$ and $A(\mathbf{k}, \omega)$ at $(0,0)$ and (π, π) points but in the opening of the gap along the boundary of the magnetic (reduced) Brillouin zone. As a result, we shall have two different bands with the periodicity of the magnetic Brillouin zone, i.e., the $(0,0)$ and (π, π) points become equivalent for each of the two bands.

APPENDIX

Chain representation and integrals over the spectral density

The integration over spectral density could be done with the quadrature approach [29], which is very efficient when applied to the electron structure calculations [32]. Unfortunately, the spectral density we deal with has no upper bound and depends exponentially on the energy; i.e., it substantially differs from the typical spectral density that appears in band-structure

calculations. It turned out that the direct application of Nex's quadrature approach [29] is not stable numerically for our purpose. For calculations of the integrals (27) we therefore use the chain representation of the continuous-fraction. This means that the continuous-fraction expansion of the form (21) may be interpreted as the Green's function $G(\omega) = \left\langle u_0 | (\omega - \hat{h})^{-1} | u_0 \right\rangle$ of the one-particle, tight-binding Hamiltonian $\hat{h}$ of the semi-infinite one-dimensional lattice with a_n, b_n, and $|u_n\rangle$ as the site energies, nearest neighbor-hoppings and on-site basis states respectively:

$$a_n = \left\langle u_n | \hat{h} | u_n \right\rangle, \quad b_{n+1} = \left\langle u_n | \hat{h} | u_{n+1} \right\rangle.$$

We introduce the eigenstates $|\psi_m\rangle$ and eigenenergies E_m of the chain Hamiltonian:

$$\hat{h} = \sum_m |\psi_m\rangle E_m \langle\psi_m|.$$

The Green's function spectral density then becomes the local density of states on the zeroth site of the chain [28]:

$$A(\omega) = -\frac{1}{\pi} \operatorname{Im} G(\omega + i0^+) = \sum_m \langle u_0|\psi_m\rangle \, \delta(\omega - E_m) \, \langle\psi_m|u_0\rangle.$$

The following identities will then hold:

$$F = \int\limits_{-\infty}^{\infty} f(\omega)A(\omega)d\omega = \int\limits_{-\infty}^{\infty} f(\omega)\sum_m \langle u_0|\psi_m\rangle \, \delta(\omega - E_m) \, \langle\psi_m|u_0\rangle \, d\omega =$$

$$= \sum_m \langle u_0|\psi_m\rangle \, f(E_m) \, \langle\psi_m|u_0\rangle = \left\langle u_0|f(\hat{h})|u_0\right\rangle. \tag{38}$$

Nex [29] has proved that for a polynomial f of the degree $2n_0 + 1$ the integral F for the infinite chain has the same value as an analogous integral for the truncated chain of length $n_0 + 1$. The Hamiltonian of the truncated chain in the basis of the states $\{|u_0\rangle \ldots |u_{n_0}\rangle\}$ has the form of the tridiagonal $(n_0 + 1) \times (n_0 + 1)$ matrix:

$$h_T = \begin{bmatrix} a_0 & b_1 & & & \\ b_1 & a_1 & b_2 & & \\ & & \cdots & & \\ & & & a_{n_0-1} & b_{n_0} \\ & & & b_{n_0} & a_{n_0} \end{bmatrix}.$$

Now, instead of integrating the spectral density function over ω, we directly calculate the matrix function $f(h_T)$ in order to take f_{00} matrix element. Then $F = f_{00}$, as follows from the last identity in Eq. (38). We see that the result for F is expressed only in terms of the first coefficients $\{a_0, \ldots, a_n, b_0 \ldots, b_n\}$.

References

1. E. Dagotto, Rev. Mod. Phys. **66**, 763 (1994).
2. S. Schmitt-Rink, C. M. Varma, and A. E. Ruchenstein, Phys. Rev. Lett. **60**, 2793 (1988); F. Marsiglio, A. E. Ruchenstein, S. Schmitt-Rink, and C. M. Varma, Phys. Rev. B **43**, 10882 (1991).
3. C. L. Kane, P. A. Lee, and N. Read, Phys. Rev. B **39**, 6880 (1989).
4. G. Martinez and P. Horsch, Phys. Rev. B **44**, 317 (1991).
5. Z. Lui and E. Manousakis, Phys. Rev. B **44**, 2414 (1991); **45**, 2425 (1992).
6. A. Sherman and M. Schriber, Phys. Rev. B. **48**, 7492 (1993); **50**, 12887 (1994); **50**, 6431 (1994).
7. N. M. Plakida, V. S. Oudovenko, and V. Yu. Yushankhai, Phys. Rev. B **50**, 6431 (1994).
8. A. Ramsak and P. Prelovsek, Phys. Rev. B **42**, 10415 (1990).
9. V. J. Emery, Phys. Rev. Lett. **58**, 2794 (1988).
10. V. J. Emery and G. Reiter, Phys. Rev. B **38**, 4547 (1988).
11. O. F. de Alcantara Bonfim and G. F. Reiter, in *Proceedings of the Univ. of Miami Workshop on Electronic Structure and Mechanisms for High-Temperature Superconductivity,* ed. by J. Ashkenazi, Plenum Press, New York (1991).
12. V. V. Kabanov and A. Vagov, Phys. Rev. B **47**, 12134 (1993).
13. O. A. Starykh, O. F. de Alcantara Bonfim, and G. F. Reiter, Phys. Rev. B **52**, 12534 (1995).
14. F. C. Zhang and T. M. Rice, Phys. Rev. Lett. B **37**, 3759 (1988).
15. A. F. Barabanov, L. A. Maksimov, and G. V. Uimin, Pis'ma Zh. Exp. Teor. Fiz. **47**, 532 (1988) [JETP Lett. **47**, 622 (1988)]; Zh. Exp. Teor. Fiz. **96**, 655 (1989) [JETP **69**, 371 (1989)]; A. F. Barabanov, R. O. Kuzian, and L. A. Maksimov, J. Phys. Cond. Matter **3**, 9129 (1991).
16. J. G. Tobin, C. G. Olson, C. Gu et al., Phys. Rev. B **45**, 5563 (1992).
17. K. Gofron, J. C. Campuzano, H. Ding et al., J. Phys. Chem. Sol. **54**, 1193 (1993).
18. A. A. Abrikosov, J. C. Campuzano, and K. Gofron, Physica C **214**, 73 (1993).
19. D. S. Dessau, Z.-X. Shen, D. M. King et al., Phys. Rev. Lett. **71**, 2781 (1993).
20. D. M. King, Z.-X. Shen, D. S. Dessau et al., Phys. Rev. Lett. **73**, 3298 (1994).
21. A. F. Barabanov, V. M. Berezovsky, E. Žasinas, and L. A. Maksimov, Zh. Eksp. Teor. Fiz. **110**, 1480 (1996) [JETP **83**, 819 (1996)].
22. H. Shimahara and S. Takada, J. Phys. Soc. Jap. **60**, 2394 (1991).
23. A. Barabanov and O. Starykh, J. Phys. Soc. Jap. **61**, 704 (1992); A. Barabanov and V. M. Berezovsky, Zh. Exp. Teor. Fiz. **106**, 1156 (1994) [JETP **79**, 627 (1994)].
24. A. F. Barabanov, R. O. Kuzian, and L. A. Maksimov, Phys. Rev. B **55**, 4015 (1997).
25. H. Mori, Prog. Theor. Phys. **33**, 423 (1965); **34**, 399 (1965).
26. N. M. Plakida, Phys. Lett. A **43**, 481 (1973).
27. J. R. Schrieffer, J. Low. Temp. Phys. **99**, 397 (1995).
28. R. Haydock in: *Solid State Physics* **35**, ed. by H. Ehrenreich, F. Seitz, and D. Turmbull, Academic Press, New York (1980).
29. C. M. M. Nex, J. Phys. A: Math. Gen. **11**, 653 (1978).
30. R. Haydock and C. M. M. Nex, J. Phys. C: Solid State Phys. **18**, 2235 (1985).
31. *The Recursion Method and its Applications*, ed. by D. G. Pettifor and D. L. Weaire, Springer, Berlin (1985).
32. R. Haydock and C. M. M. Nex, J. Phys. C: Solid State Phys. **17**, 4783 (1984).
33. *Handbook of Mathematical Functions*, ed. by M. Abramowitz and I. A. Stegun, Nat. Bur. of Standards (1964).
34. A. P. Kampf and J. R. Schrieffer, Phys. Rev. B **42**, 7967 (1990).
35. W. Marshall, Proc. R. Soc. London Ser. A **232**, 48 (1955); E. Lieb and D. C. Mattis, J. Math. Phys. **3**, 749 (1962).